Colloids and Surfaces A: Physicochemical and Engineering Aspects 700 (2024) 134695

Contents lists available at ScienceDirect

Colloids and Surfaces A: Physicochemical and Engineering Aspects

journal homepage: www.elsevier.com/locate/colsurfa

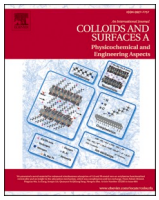

Chitosan electrolyte hydrogel with low ice adhesion properties

Irene Tagliaro [*,1], Veronica Radice [1], Roberto Nisticò, Carlo Antonini [*]

Department of Materials Science, University of Milano-Bicocca, via Cozzi 55, Milano 20131, Italy

GRAPHICAL ABSTRACT

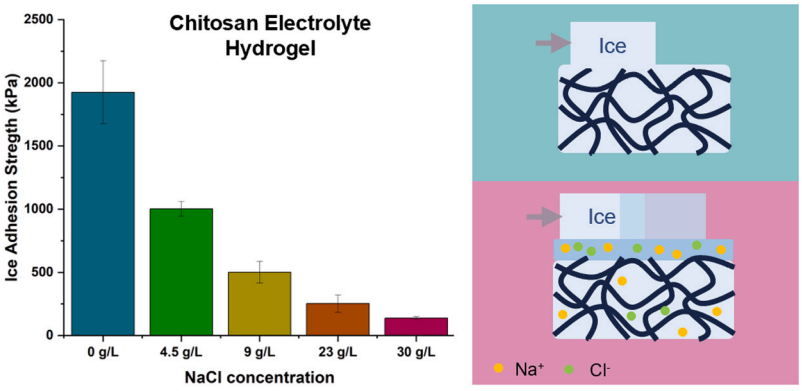

ARTICLE INFO

Keywords:
Chitosan hydrogel
Electrolyte
Salt-infused
Low ice adhesion

ABSTRACT

Icephobic materials can prevent or reduce ice formation, e.g. by ensuring easy detachment, a desirable property for those applications where ice accumulation is critical to human safety. Herein, we develop a chitosan electrolyte hydrogel to create a bio-based surface with low ice adhesion. The chitosan electrolyte hydrogel is physically crosslinked and infused with salted water at concentrations from 4.5 to 30 g/L, including that of seawater (23 g/L). Depending on salt content in the hydrogel, we could obtain very low ice adhesion down to 140 kPa (at – 10°C). We hypothesize that the chitosan electrolyte hydrogel exploits the colligative properties of water avoiding the ice nucleation at the ice-hydrogel interface. To confirm the hypothesis, we investigate the chitosan electrolyte hydrogel structure by contact angles analysis, DSC, TGA, FTIR, XRD, and by rheometry for mechanical properties. We quantify the presence of non-freezing water, which creates a lubricating liquid water layer at the ice-hydrogel interface, affecting the ice detachment mechanism and lowering ice adhesion. In conclusion, the proposed chitosan electrolyte hydrogel presents a bio-based and cost-efficient strategy for ice detachment across various icing scenarios for systems operating in humid marine environments, such as offshore platforms and ships.

* Corresponding authors.
E-mail addresses: irene.tagliaro@unimib.it (I. Tagliaro), carlo.antonini@unimib.it (C. Antonini).
[1] Irene Tagliaro and Veronica Radice contributed equally to this work.

https://doi.org/10.1016/j.colsurfa.2024.134695
Received 19 April 2024; Received in revised form 4 June 2024; Accepted 2 July 2024
Available online 3 July 2024

1. Introduction

Ice formation and adhesion on surfaces pose significant challenges for various applications, such as aviation, transportation, energy, and civil engineering, where they can impair performance, increase drag, and cause hazard to humans [1-3]. Icephobic materials are studied as passive strategies to inhibit or delay ice nucleation and growth reducing ice adhesion on their surfaces for easy removal [4,5]. A common strategy to develop icephobic materials is to enhance their hydrophobicity, relying on the reduction of the contact area with water [6]. However, in high humidity conditions, superhydrophobic surfaces often results in high ice accretion when water penetrates the roughened textures, calling for the development of innovative methods to ensure effective ice prevention [7]. One similar route is to infuse the surface with a liquid immiscible to water, the so-called slippery lubricant-infused surfaces (SLIPS) or Lubricant-Infused Surfaces (LIS)[8]. Opposite approaches exploit the hydrophilic properties of materials, where the formation of a water liquid layer on the surface can make the ice slide [9,10]. In this case, surfaces are infused with a hydrophilic lubricating liquid which create a composite solid−lubricant−water which may inhibit the formation of ice and lower ice adhesion [11]. Hydrophilic materials are frequently found in the form of gels, inherently soft materials, which can also help in reducing ice adhesion [12]. Hydrophilic gels are particularly interesting for their ability to absorb fluids such as cryoprotectants or solutes creating a slippery surface [13-18]. Whitin this frame, polysaccharides stand out as they are soft hydrophilic absorbent materials, which combine biodegradability and non-toxicity. In nature, we find examples of how polysaccharide gels can protect microorganisms which live in extreme conditions, such as diatoms, typical Arctic ice algae, exploiting the protective environment of polysaccharide gels and comprising the concentration of solutes with non-colligative effects of water biding polysaccharides [19,20]. Since polysaccharides possesses high adsorption and water-binding capacity, we may differentiate between free and bound water. Bound water can be further categorized into tightly bound (non-freezable water) and loosely bound, which has more mobility and can freeze below 0°C [21]. The presence of bound-water states impacts on the formation of a liquid water layer at the ice-surface interface inhibiting the formation of ice crystals and increasing the mobility of ice on hydrated surfaces [22]. The increased concentration of ions, moreover, lowers the freezing point, contributing to the increase of the liquid water total amount.

In the field of conductive sensors, polysaccharide hydrogels have been studied as soft-wet materials with a crosslinked structure able to retain water and solutes [23,24]. Cellulose-based hydrogels infused with different salts are found to maintain good conductivity at −30 °C [25]. Durable sensors of cellulose hydrogels with good mechanical properties are often derived from a double crosslinking comprising covalent and ionic binding [26,27]. Similarly, a dextran hydrogel with high concentration of sulfate and ammonium ions can maintain its conductivity at −30 °C [28], while a chitosan-glycerol hydrogel until −50 °C [29]. These polysaccharide-based hydrogels show promising results for the maintenance of their performances as sensors at low temperatures but have never been investigated systematically in their icephobic and ice adhesion properties. Exploiting the properties of binding water molecules, hydrophilic polysaccharides have been crosslinked with dopamine creating a hyaluronic acid surface with low ice adhesion (65 kPa) [30] and a sodium alginate hydrogel, which inhibits ice nucleation down to −23 °C [31]. Still, polysaccharide hydrogels are sometimes deficient in mechanical performances and usually do not withstand high strain deformation [32]. To overcome this issue, a physically crosslinked hydrogel of chitosan can be obtained from dissolution in basic environment and crosslinked in mild conditions [33]. While dissolution in acidic conditions typically leads to hydrogels with poor mechanical strength [34], the advantage of this basic dissolution procedure is the obtainment of a strong physical crosslink among chitosan polymeric chains which does not require the addition of chemical crosslinkers [35, 36]. Chitosan is an abundant polysaccharide, which combines biodegradability [37] and non-toxicity [38] with the possibility to easily modify [39-41] and exploit its functional groups for physical crosslinking. Additionally, its hydrogel structure can retain high amount of water and is able to withstand considerable deformation, as already demonstrated elsewhere [34,35].

Therefore, in this study, we explore the icephobicity properties of a physically crosslinked chitosan matrix infused with NaCl solutions spanning from 4.5 to 30 g/L, including that of seawater (approx. 23 g/L). Due to the presence of ions which are retained by the polysaccharide network, the electrolyte chitosan hydrogel allows the formation of a water liquid layer at the interface between the ice and the hydrogel surface, thus decreasing the ice adhesion strength. In this simple and economic system, we oserve a combined effect on icephobicity deriving from colligative (i.e. electrolyte solution) and non-colligative properties (i.e water molecules binding of the polysaccharide hydrogel) by DSC and contact angle analysis. Furthermore, we also characterize the hydrogel evaluating the physicochemical properties and the rheology. Moreover, the chitosan electrolyte hydrogel (CEH) combines biodegradability, low-cost, non-toxicity and the possibility of easily replenishing the salt solutions with available ion sources, when applied in marine environment, thus making it potentially suitable in offshore platforms and ships.

2. Materials and methods

2.1. Materials

Chitosan powder low molecular weight (Mw)(LMw)(DD 76 %, Mw 50.000–190.000 Da, CAS 9012–76–4), Chitosan powder high (HMw) (DD 76 %, Mw 310.000–375.000 Da, CAS 9012–76–4), and Sodium Hydroxide tablets (NaOH, CAS 1310–73–2) purchased from Merck KGaA. Sodium Chloride crystalline powder (NaCl, 99+%, CAS 7647–14–5) purchased from ThermoFisher (Kandel) GmbH.

2.2. Preparation of the chitosan electrolyte hydrogel

The preparation of the CEH starts with the dissolution of chitosan in basic environment at low temperature [33,36]. High and low molecular weight chitosan (76 % DD) in the ratio 70:30 respectively (26 g/L of HMw chitosan and 11 g/L of LMw chitosan) are mixed in 27 mL of a NaOH 2.1 M solution (Fig. 1a). The dispersion is mixed for 1 hour at room temperature (Fig. 1b). The mixture is then transferred to a refrigerator and stored overnight at – 20 °C to obtain a frozen solution of chitosan (Fig. 1c). The day after the frozen solution is removed from the refrigerator and gently stirred, inducing its gradual thawing (Fig. 1d). 5 g of the thawed transparent solution (Fig. 1e') are poured into a 5 cm diameter Petri dish (Fig. 1e) and cured it in the oven at 45 °C for 5 min to create a hydrogel film on the surface. This step is done to prevent dissolution and creation of uneven surfaces on the hydrogel that can often occur when suddenly immersed in the water bath described in the next step. The hydrogel in the Petri dish is immersed in a thermal bath at 45 °C for 1 hour (Fig. 1 f). The thermal bath consists of 700 mL of aqueous solution with the desired NaCl concentration (0 g/L, 4.5 g/L, 9 g/L, 23 g/L, 30 g/L). During this step the transparent solution undergoes a sol–gel transition on heating with the formation of a hydrogel (Fig. 1 f'). The jellified solution is repeatedly washed in 200 mL of neutral aqueous solution with a desired saline concentration until the pH of the hydrogel reaches neutrality (pH = 7) (Fig. 1 g and g'). The samples are tested in a custom-built horizontal shear test set-up (Fig. 1 h). When exposed to temperatures below 0°C the gel become opaque (Fig. 1 h').

The hydrogels are purely made by a physical cross-linked chitosan, without the addition of any curing agent or additive [33]. Indeed, the preparation procedure exploits the dissolution at low temperatures of an alkali-chitosan mixture which is cured under mild conditions, as already studied for chitosan [36], and cellulose [42], usually involving the

presence of urea. This dissolution method does not involve the protonation of amine groups, as usually done by the addition of acids, such as 1–5 % acetic acid solution [32,38], but rather exploit the disruption effect of Na^+ ions on NH—O═C intermolecular hydrogen bonds and NH—O6 hydrogen bonds of chitosan [43]. Therefore, to obtain good dissolution with NaOH, it is of great importance to use chitosan with a DD% up to ca. 75 % [44]. The sol-gel transition in a water bath at 45°C is attributed to a change in the solubility of the medium. The chitosan dissolution complex containing Na^+ ions collapse in hot water and chitosan loses its solubility. Therefore, the chitosan polymeric chains crosslink with the formation of a physical network [45,34,46]. After repetitive washings, this procedure provides a pure chitosan hydrogel, which is a very simple environmental-friendly soft material that can load NaCl solution, for creating a low ice-adhesion material.

2.3. Methods

The ice adhesion test is performed using an own custom-built horizontal shear test set-up [47]. The core of the instrument is placed inside a transparent environmental chamber to guarantee a close atmosphere; the humidity inside the chamber is controlled by a hygrometer and nitrogen flow (RH < 2 %) to avoid uncontrolled frost formation during the experiments. The cooling process is managed by a thermoelectric cooling system (Peltier cells) located under a metal stage where the samples are placed to reach the desired freezing temperature. The temperature difference within the Peltier cells is regulated through a circuit board (RS-00 777 C; RS – 00849) that can modulate the current output and, consequently, the temperature difference in the Peltier cell according to the so–called Peltier effect, cooling down the top surface, whereas the Peltier bottom (hot) side is in contact with a heat exchanger where liquid water circulates at 3 ° - 5 °C, refrigerated with a chiller (Thermo-Scientific ThermoChill II Recirculating Chiller). The pushing height, at which the external force is applied on the ice block (Fig. 1 h) is h = 2 mm. The ice adhesion strength is measured by a dynamometer (Mark-10, Force Gauge Model M5–20) placed over a trolley with controlled movement. Ice is formed inside a cylinder mold with diameter of 8 mm filled with 7 drops (0.35 mL) of deionized water. The freezing process occurs within 15 minutes when setting the surface temperature in the range −10 °C to −20 °C. The measurement is performed right after the freezing process and the dynamometer is moved forward at 0.01 mm/s speed and the load (N) vs time (s) graph is obtained. The measurement of temperature is performed with a thermocouple on the surface of the sample and kept constant thought the entire procedure. Each point in the ice adhesion graphs is an average of 3 measurements conducted on different samples.

The contact angle analysis is performed using an in-house contact angle setup, consisting of a camera (Fastcam Nova S6, Photron) and backlight illumination. Static contact angle is measured infusing deionized water with a syringe pump (Harvard Apparatus, Pump 11 Pico Plus Elite) at a rate of 10 μL/min, with drop volumes in the range of 7–10 μL. Advancing, θ_A, and receding, θ_R, contact angles are measured dispensing and withdrawing deionized water with the same syringe pump with a four step procedure: i) water infusion of an initial 3 μL drop at a rate of 10 μL/min, ii) delay 3 s to enable vibration damping, iii) water infusion at a rate of 10 μl/min (5 μL, final total volume of 8 μL), iv) water withdrawal at a rate of 10 μl/min (8 μL). A video is recorded

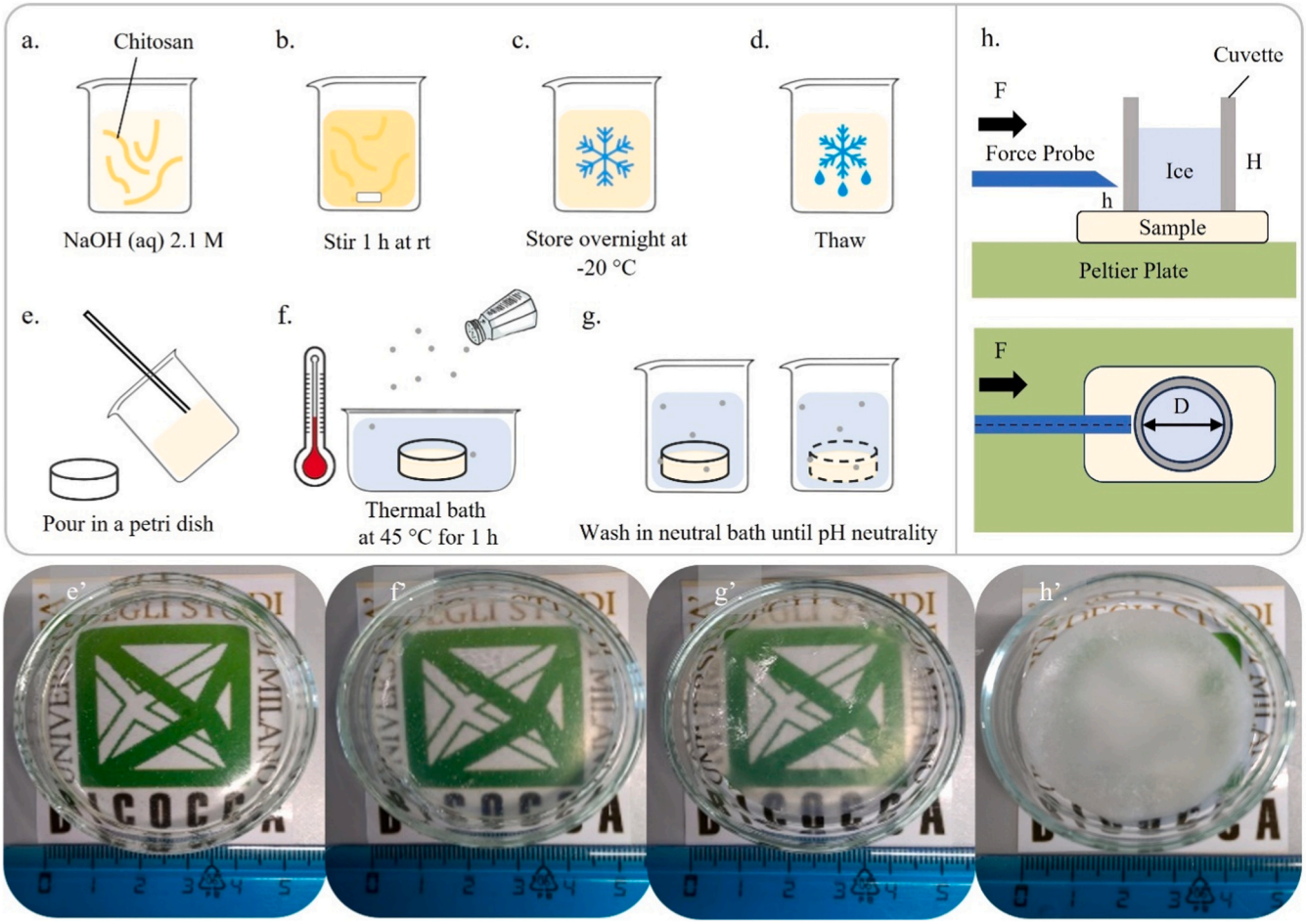

Fig. 1. a – g) Schematic representation of the CEH preparation; h) schematic of custom-built horizontal shear test set-up during the ice adhesion test; e'– h') pictures of CEHs at the corresponding preparation step.

using the software Photron Fastcan Viewer, PFV4. To analyze the video, DropenVideo, an open-source software developed in MATLAB is used [48]. Every point in the contact angle graphs is average of three measurements performed on one sample.

X-Ray diffraction analysis (XRD) is performed using a Rigaku Miniflex 600, a benchtop powder X-ray diffractometer with a Bragg-Brentano (θ - 2θ) parafocusing geometry. The instrument is operated at the maximum power 600 W (40 kV – 15 mA). The hydrogels are measured in their wet and dry form. The acquisition has angle range of 5° to 80° at a speed of 5°/min with steps of 0.01°.

Rheology measurements are performed with Anton Paar Modular Compact Rheometer (MCR) 92 using a parallel plate geometry with plate diameter equal to 5 cm. The hydrogels are measured with a gap of 4 mm between the parallel plates. Strain sweep tests are performed from 0.1 % to 100 % strain at 10 Hz. Frequency sweep tests are collected with 1 – 50 Hz at 1 % strain.

The Fourier Transform Infrared spectroscopy (FTIR) analysis is performed using a ATR Thermo Fisher Scientific Nicolet™ iS20 FTIR Spectrometer with spectral range 500–4000 cm^{-1}, 28 scans, 4 cm^{-1} resolution).

For the Differential Scanning Calorimetry (DSC) analysis a Mettler Toledo DSC3 STARe system is used. The temperature program performed is the following: i) temperature decrease from 25 °C to −40 °C at 10 °C/min, ii) constant temperature at −40 °C for 2 min, iii) temperature increase from −40 °C to 25 °C at 10 °C/min. By DSC analysis, it is possible to calculate the freezable W_f and non-freezable water W_{nf} fractions contained in the hydrogels. The content of the freezable water W_f can be calculated as:

$$W_f = \frac{\Delta H_f}{\Delta H_0} \quad (1)$$

where ΔH_f is the melting enthalpy of freezable water, ΔH_0 is the standard enthalpy of fusion of pure water with values of 324 (J/g)[49]. Both ΔH are obtained as integration of the melting peak of the DSC curves, obtained dividing the function of heat (mW) by the weight of water (mg) inside the chitosan electrolyte hydrogel. The total content of water W_c in the hydrogels has been previously determined by gravimetric analysis [50]. The samples are weighted before (M_{tot}) and after (M_{dry}) oven drying treatment at 100 °C for 2 h, for reaching the complete evaporation of water.

$$W_c = 1 - \frac{M_{dry}}{M_{tot}} \quad (2)$$

The W_{nf} content is therefore determined by:

$$W_{nf} = W_C - W_f \quad (3)$$

Thermogravimetric analysis (TGA) is performed using a Mettler Toledo TGA/DSC 1 STAR System. The samples are heated from 30°C to 1000°C at 10 °C/min, in air flux of 50 mL/min, in standard alumina pans (capacity 70 μL). By TGA analysis, we could confirm the NaCl content inside CEH, by subtracting the percentual decomposition in weight of chitosan in pure CEH degradation curve from that of CEH containing salts.

A corrosion test on stainless steel has been performed on a Stainless-Steel foil (Stainless Steel Foil, π PI-KEM, Unit 18–20 Tame Valley Business Centre, Magnus, Tamworth, B77 5BY, UK). The chitosan electrolyte hydrogel is made in contact with the steel surface for 1 h. Steel and hydrogels in contact are put in a refrigerator at −20 °C for 1 night and finally thawed.

3. Results and discussion

CEH with different concentrations of NaCl solutions (0 g/L, 4.5 g/L, 9 g/L, 23 g/L, 30 g/L) are prepared, including the value corresponding to a physiological solution (approx. 9 g/L) and seawater (approx. 23 g/L) (Fig. 1). Our hypothesis is that the combination of a soft material and a hydrophilic sponge containing salt ions would be beneficial for obtaining low ice adhesion due to the change of the colligative properties of water during the ice-adhesion tests (Fig. 1 h and h'), preventing the ice nucleation at the ice-hydrogel interface. The hypothesis is tested against material characterization results reported here below.

Fig. 2 shows the ice adhesion tests on CEH with increasing salt contents at different temperatures. In Fig. 2a, CEH with 0 g/L, 4.5 g/L, 9 g/L, 23 g/L, 30 g/L are tested in their ice adhesion properties at −10°C and −20°C. At −10°C, we observe a strong decrease in the ice adhesion strength from 1924 kPa for 0 g/L to 138 kPa for 30 g/L. This effect is remarkable considering the comparison with aluminum (1200 kPa ± 20) and glass (1500 kPa ± 9) reference substrates, ice adhesion is reduced up to a factor 10. The same trend is preserved at −20°C where ice adhesion strength is 2002 for 0 g/L and 477 kPa for 30 g/L. The decrease in ice adhesion strength is therefore connected to the salt concentration, which can maintain a thin layer of liquid water at the interface with the ice block. This effect is more evident at −10°C since more water is presumably maintained in its liquid form. The preservation of lubricating liquid water can be inferred by the force profiles recorded in time during the ice adhesion experiments (Fig. 2b). From CEH with 0 g/L to 30 g/L, together with the decrease of the maximum force, we can observe the consistent change of the curve profile. CEH with 0 g/L (blue line) has a very sharp detachment, while the other samples switch consistently to smoother peaks. This trend is due to a combined effect of increasingly slippery surface and decreasingly hard substrate from 0 to 30 g/L. With increasing salt concentration, the hydrogel changes therefore its mechanical properties ensuring smoother and easier detachment of ice. The same effect is appreciable with the decrease of temperature in different ice adhesion tests. Fig. 2c shows the ice adhesion strength for a CEH of 23 g/L measured at decreasing temperature. Also in this case, we observe an almost linear increase of ice adhesion strength for decreasing temperatures, from 264 kPa at −10 °C to 913 kPa at −22 °C. This trend has been attributed to the increase of frozen water, as also confirmed by the force profiles in Fig. 2d. The curves are sharper at −22 °C (dark blue line) and smoother at lower temperatures, showing the increased softness and slippery surface of samples. The force profile at −22 °C (dark blue line) shows a double peak which is the effect of ice second time adhesion with the surface after the first detachment. This is consistently observed in repeated experiments. Also, ice adhesion properties are verified by testing at −10 °C each CEH at different salt concentration over repeated cycles on the same sample (Figure S1a) and in time frame of 50 days (Figure S1b).

The CEH are studied in their physicochemical and surface properties to understand correlations with ice adhesion results. Samples are investigated by quasi-static contact angle (Fig. 3a) to understand the impact of surface wettability. In Fig. 3a, CEHs show hydrophilic wetting properties with a θ_A that decrease from 102° ± 8 at 0 g/L to 42° ± 13 at 30 g/L; for all surfaces, θ_R<20° (the exact value is difficult to measure for very low contact angle). The obtainment of very high hysteresis ($\Delta\theta = \theta_A - \theta_R$) is typical of hydrophilic materials. Moreover, the increase of salt results in higher hydrophilicity of the surface. This effect is further confirmed by static contact angle analysis (Figure S2a) where the angle decreases from 89° to 29° at high salt content. The values of static contact angles for CEH with no salt are in agreement with the literature on chitosan hydrogels [51]. The evolution of static contact angle is evaluated in a time frame of 10 minutes (Figure S2b), showing a slight increase in hydrophilicity of around 5° over time at all salt concentrations. The increased hydrophilicity of CEH with high salt concentration is correlated to the increased Coulomb attraction between water and substrate, enhanced by increased numbers of hydrogen bonds [52]. Hence, we observe that the more hydrophilic samples have the lowest ice adhesion (Fig. 2a). This is an effect rarely reported in the literature, where higher hydrophobicity is usually connected to lower ice adhesion [53,54]. Thus, we hypothesize that, the water molecules interact through hydrogen bonds with the polysaccharide hydroxyls and NaCl

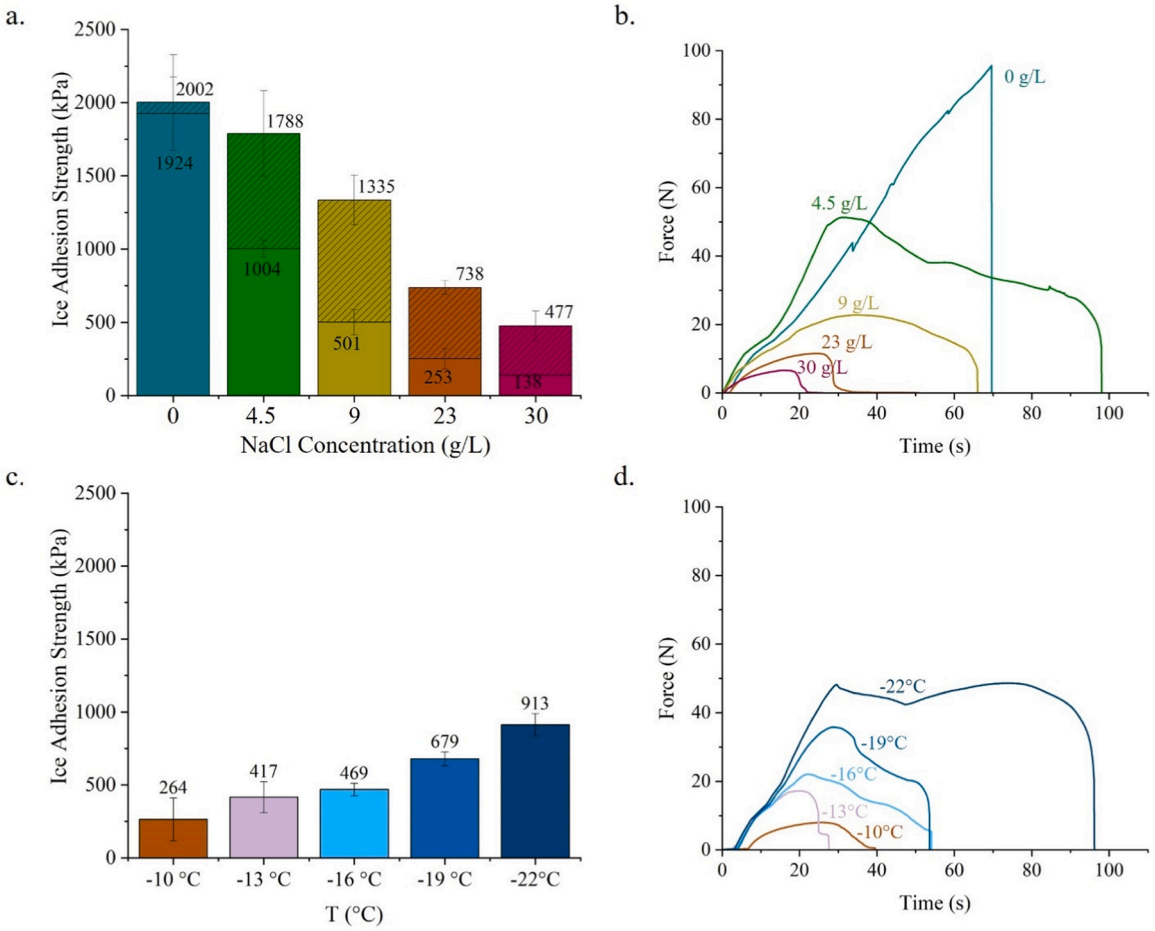

Fig. 2. a) Ice adhesion strength on CEH at different electrolyte concentrations measured at −10 °C (solid columns), −20 °C (striped columns) with 0 g/L (blue column), 4.5 g/L (green column), 9 g/L (yellow column), 23 g/L (orange column), 30 g/L (magenta column); b) force profile recorded during the ice adhesion measurement at −10 °C for CEH 0 g/L (blue line), CEH 4.5 g/L (green line), CEH 9 g/L (yellow line), CEH 23 g/L (orange line), CEH 30 g/L (magenta line); c) ice adhesin strength of CEH 23 g/L at different temperatures −10 °C (orange column), −13 °C (purple column), −16 °C (light blue column), −19 °C (blue column), −22°C (dark blue column); d) force profile of CEH 23 g/L recorded at different temperatures −10 °C (orange line), −13 °C (purple line), −16 °C (light blue line), −19 °C (blue line), −22 °C (dark blue line).

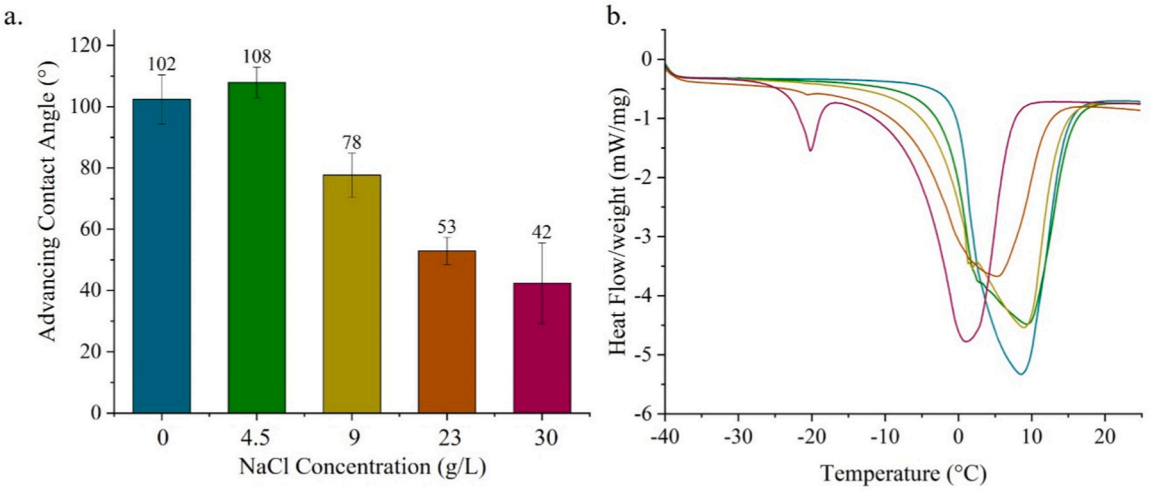

Fig. 3. a) Quasi-static contact angle analysis of CEH. θ_A of CEH with 0 g/L (blue column), 4.5 g/L (green column), 9 g/L (yellow column), 23 g/L (orange column), 30 g/L (magenta column). θ_R is $< 20^\circ$ for each sample; b) DSC endothermic profiles of chitosan electrolyte hydrogels at increasing T with 0 g/L (blue line), 4.5 g/L (green line), 9 g/L (yellow line), 23 g/L (orange line), 30 g/L (magenta line).

ions, slowing down the ice formation process near the surface.

By DSC analysis, we investigate the water phase transition from liquid to ice in the hydrated polymeric network of hydrogels. Fig. 3b shows the evolution of the T_m for the CEH at the different salt concentrations at increasing T. A decrease of the T_m with the increase of salt content (Table 1), from 9.8 °C at 0 g/L to 2.3 °C at 30 g/L is observed [55]. At 4.5 and 9 g/L, we appreciate the presence of a shoulder in the T_m peak toward lower temperatures, while for 23 and 30 g/L we observe the formation of another peak at −20 °C. A similar trend in T_m decrease is visible in DSC analysis of pure water/salt solution at the same concentrations (Figure S3a), whereas the secondary peak at −20 °C is always present in water salt solutions. The endothermic peak at −20 °C is attributed to the melting of the eutectic mixture of ice and NaCl [56], which is not visible in the case of CEH 9 and 4.5 g/L. This is probably due to the biding of ions with chitosan [57]. The DSC analysis shows an exothermic peak relative to freezing (Figure S3b) at decreasing temperature. The freezing temperature of CEH with no salt is −10°C, while −12°C for all salt concentration of CEH.

Since the area of the T_m peak represents the enthalpy associated with the melting of freezing water, by knowing the water content of the hydrogel (assessed gravimetrically and confirmed by TGA, see Table S1), it is possible to estimate the content of freezable and non-freezable water, considering that the enthalpy quantified by DSC is only associated only to the W_f (Table 1). With no salt, the CEH show 0.05 of W_{nf} which imply the presence of water in a tightly bounded state by hydrogen interaction with the chitosan polymeric structure. The decrease of ΔH_0 at higher salt concentration corresponds to the decrease of W_f and the consequent increase of W_{nf} up to 0.25 in the case of 30 g/L. The presence of salt seems to increase bounding of chitosan polymeric chains with water. A higher content in W_{nf} is in agreement with the ice adhesion trend, as lower ice adhesion is measured at higher salt content. Therefore, the presence of W_{nf} plays a role in maintain a lubricating liquid layer at the ice-hydrogel interface, lowering ice adhesion at higher salt concentrations.

In the FTIR spectra of the CEH (Fig. 4a), we can appreciate the signals of chitosan. The strong band at 3290–3360 cm^{-1} is ascribed to N-H and O-H stretching, while at 2920 and 2870 cm^{-1} to C-H symmetric and asymmetric stretching, respectively. At 1645 and 1560 cm^{-1}, we observe the bands related to the acetyl groups, respectively attributed to stretching of CO and bending of NH. The symmetric bending of CH_2 and CH_3 is visible at 1420 and 1375 cm^{-1} and the CO stretching at 1063 and 1025 cm^{-1} [58]. No significative difference is visible in the FTIR spectra among different salt concentrations.

In Fig. 4b, we report the XRD diffraction wet CEH. The broad peaks at ca. 28° 2θ and ca. 41° 2θ belongs to the diffraction of liquid water, while the small peak at 20° 2θ is attributable to the (110) reflection of the crystalline chitosan [34,36]. No significant differences are observed in the change of crystallinity among different quantities of salts. The same diffraction pattern is also appreciable after freezing at −20 °C and thawing (Figure S4), proving the crystallinity is not altered after the temperature change. The dry samples show only the diffraction pattern of NaCl (Figure S4).

The thermal decomposition of CEH is studied by TGA (Fig. 4c). The first step between 30 and 200°C is related to the evaporation of water which is ca. 10 wt% in the case of CEH with no salt and to ca. 5 wt% at all salt concentrations. The second step between 200 and 750°C is due to the decomposition of chitosan. While in the case of CEH with no salt (blue line) decomposition of CEH is complete at 750°C, in the case of CEH samples with salt we appreciate a last step due to NaCl melting. As such, it is confirmed that the quantity of NaCl in CEH corresponds to the nominal concentration of the solutions (Table S1).

The mechanical properties of the CEH are studied by performing rheology analysis (Fig. 4d) varying either the frequency sweep (in the 1–50 Hz range at 1 % strain) or the strain amplitude (in the 0.1–100 % strain range at 10 Hz of frequency). Since similar performances are obtained over the different samples, curves are average values of all CEH tested. As reported in the graph showing the frequency dependence of the G' and G'' moduli (Fig. 4d, top), once the CEH is formed, G' is always higher than G'', and both moduli are independent from the frequency range investigated, with absence of a crossover frequency, thus suggesting that the hydrogel network is mechanically robust and behaves as a viscous solid throughout the entire test [59,60]. In the case of the graph showing the strain dependence of the G' and G'' moduli (Fig. 4d, bottom), instead, it has been registered a more complex behavior. In fact, in the low strain region, both the G' and G'' are almost constant, whereas by increasing the strain amplitude the G' and G'' curves intersect at a strain of *ca*. 22 % (extrapolated value), which is the critical strain value indicating the transition of the gel network to a liquid state. A further increment of the strain to 100 %, instead, causes a decrease of both G' and G'' values, probably due to the collapse of the CEH network [61,62].

To confirm the possibility of applying the hydrogels on surfaces without causing any oxidation/degradation, we conducted a test by depositing CEH on stainless steel sheets and freeze and thaw the materials at all concentration of salts (4.5, 9, 23, 30 g/L). The samples were frozen overnight and thawed the day after (total time of contact 12 h). No effects of corrosion are visible (Figure S5).

We assessed the stability of CEH with no salt for 1 week at different pHs. Figure S6a,b shows that the hydrogel is well maintained after 1 week at pH 9, while, in the case of pH 4, the hydrogel looks swollen after 24 h, and it is partially dissolved after 1 week at pH 4. Therefore, this experiment limits the applicability of CEH at acidic pHs.

Table 1
Results from DSC analysis of T_m, temperature of melting; ΔH_0, enthalpy associated with the melting of freezing water; W_c is the water total content, W_f and W_{nf}, freezable and non-freezable water content.

Sample NaCl (g/L)	T_m (°C)	ΔH_0 (J/g)	Wc	W_f	W_{nf}
0	9.8 ± 1.9	290 ± 10	0.950 ± 0.006	0.90 ± 0.03	0.05 ± 0.03
4.5	9.3 ± 0.1	277 ± 29	0.941 ± 0.003	0.85 ± 0.09	0.09 ± 0.09
9	9.3 ± 0.5	268 ± 24	0.937 ± 0.003	0.83 ± 0.07	0.11 ± 0.07
23	5.4 ± 0.4	229 ± 6	0.922 ± 0.005	0.71 ± 0.02	0.22 ± 0.02
30	2.3 ± 1.8	218 ± 27	0.917 ± 0.002	0.67 ± 0.08	0.25 ± 0.08

4. Conclusion

In this study, we develop a chitosan electrolyte hydrogel as a bio-based surface with low ice adhesion. The chitosan electrolyte hydrogel is physically crosslinked and infused with different amounts of salted water from 0 to 30 g/L. We find that the salt concentration influences ice adhesion and detachment behavior. This effect is mainly due to the alteration of colligative properties, which prevents ice nucleation at the ice-hydrogel interface, ensuring the presence of a lubricating liquid water layer that reduces ice adhesion. Our results show that the chitosan electrolyte hydrogel can achieve low ice adhesion, down to 140 kPa, with a reduction of a factor 10 compared to ice adhesion on reference aluminum (1200 kPa ± 20) and glass (1500 kPa ± 9) substrates. Although surfaces with extremely low ice adhesion have been reported down to 1–10 kPa [63], we consider this result promising for a very simple system constituted simply by ~ 5 % in w/w chitosan, water and salt, since direct comparison among different ice-adhesion measurement set-ups was demonstrated not possible [64]. From ice pushing test, it is visible that the ice detachment mechanism changes from sharp detachment to sliding, suggesting the presence of a softer material and a lubricating layer. The assumption is proved by investigating the chitosan hydrogel structure and properties by various methods, such as contact angle, TGA, FTIR, XRD, rheometry, and DSC. Contact angle analysis

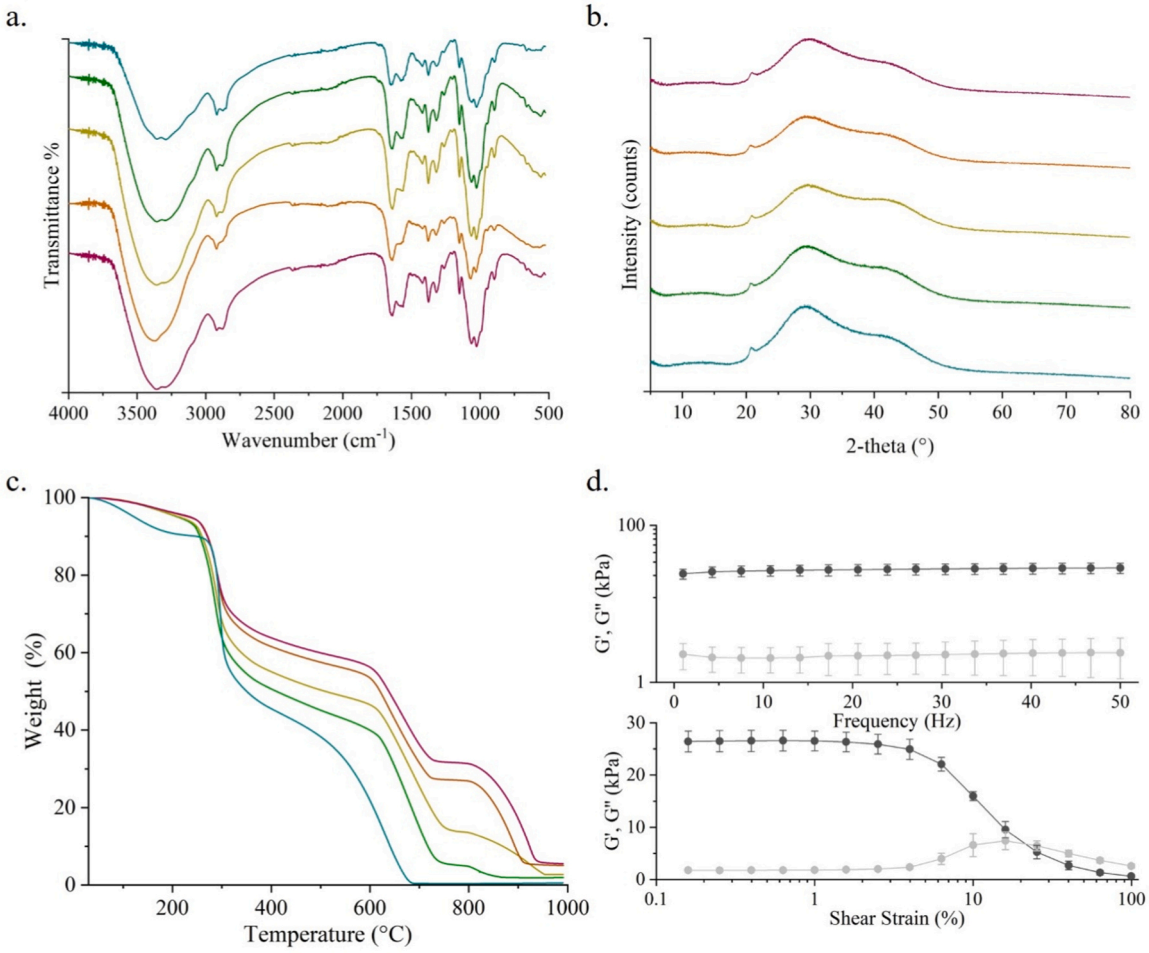

Fig. 4. a) FTIR spectra of CEH with 0 g/L (blue line), 4.5 g/L (green line), 9 g/L (yellow line), 23 g/L (orange line), 30 g/L (magenta line); b) XRD diffraction of chitosan electrolyte hydrogels with 0 g/L (blue line), 4.5 g/L (green line), 9 g/L (yellow line), 23 g/L (orange line), 30 g/L (magenta line); c) TGA analysis of chitosan electrolyte hydrogels with 0 g/L (blue line), 4.5 g/L (green line), 9 g/L (yellow line), 23 g/L (orange line), 30 g/L (magenta line); d) Frequency and Strain sweep of elastic modulus (G') and loss modulus (G'') of CEH samples mediated over the tested samples: G' (black dots) and G''(grey dots).

shows that the surfaces are increasingly hydrophilic with the increase of salt content (θ_A from 102 °C at 0 g/L to 42° at 30 g/L, $\theta_R < 20°$). DSC analysis enables the quantification of freezing and non-freezing water in the hydrogel. W_{nf} increases for increasing salt concentration, confirming that the non-freezing water acts as a lubricating layer that facilitates ice detachment. Our study introduces a bio-based and cost-efficient strategy for ensuring easy ice detachment across various icing scenarios for systems operating in marine environments. Future studies are investigating the possibility of exploiting the chitosan electrolyte hydrogel as surface coating with the application of chemical primers to covalently bound chitosan onto a desired substrate.

Funding

This project was partially funded by the European Union's Horizon 2020 research and innovation programme under the Marie Skłodowska-Curie grant agreement No 956703 (SURFICE Smart surface design for efficient ice protection and control).

CRediT authorship contribution statement

Irene Tagliaro: Writing – original draft, Supervision, Investigation, Formal analysis, Conceptualization. **Roberto Nisticò:** Writing – review & editing, Supervision. **Veronica Radice:** Writing – original draft, Investigation. **Carlo Antonini:** Writing – review & editing, Supervision, Conceptualization.

Declaration of Competing Interest

The authors declare that they have no known competing financial interests or personal relationships that could have appeared to influence the work reported in this paper.

Data availability

Data will be made available on request.

Appendix A. Supporting information

Supplementary data associated with this article can be found in the online version at doi:10.1016/j.colsurfa.2024.134695.

References

[1] T. Dimitriadis, L. Stendardo, I. Tagliaro, A.M. Coclite, C. Antonini, T. Maitra, Capillary-driven water transport by contrast wettability-based durable surfaces, ACS Appl. Mater. Interfaces *15* (22) (2023) 27206–27213, https://doi.org/10.1021/acsami.3c03840.

[2] G. Gastaldo, M. Budinger, Y. Rafik, V. Pommier-Budinger, V. Palanque, A. Yaich, Full instantaneous de-icing using extensional modes: the role of architectured and multilayered materials in modes decoupling, Ultrasonics *138* (2024), https://doi.org/10.1016/j.ultras.2024.107264.

[3] I. Tagliaro, A. Cerpelloni, V.M. Nikiforidis, R. Pillai, C. Antonini, On the development of icephobic surfaces: Bridging experiments and simulations. In The Surface Wettability Effect on Phase Change, Springer International Publishing, 2021, pp. 235–272, https://doi.org/10.1007/978-3-030-82992-6_8.

[4] K. Golovin, S.P.R. Kobaku, D.H. Lee, E.T. DiLoreto, J.M. Mabry, A. Tuteja, Designing durable icephobic surfaces, Sci. Adv. *2* (3) (2016), https://doi.org/10.1126/sciadv.1501496.

[5] G. Hernández Rodríguez, M. Fratschko, L. Stendardo, C. Antonini, R. Resel, A. M. Coclite, Icephobic gradient polymer coatings deposited via iCVD: a novel approach for icing control and mitigation, ACS Appl. Mater. Interfaces *16* (9) (2024) 11901–11913, https://doi.org/10.1021/acsami.3c18630.

[6] A.J. Meuler, J.D. Smith, K.K. Varanasi, J.M. Mabry, G.H. McKinley, R.E. Cohen, Relationships between water wettability and ice adhesion, ACS Appl. Mater. Interfaces *2* (11) (2010) 3100–3110, https://doi.org/10.1021/am1006035.

[7] H.A. Stone, Ice-phobic surfaces that are wet, ACS Nano *6* (8) (2012) 6536–6540, https://doi.org/10.1021/nn303372q.

[8] W.S.Y. Wong, K.I. Hegner, V. Donadei, L. Hauer, A. Naga, D. Vollmer, Capillary balancing: designing frost-resistant lubricant-infused surfaces, Nano Lett. *20* (12) (2020) 8508–8515, https://doi.org/10.1021/acs.nanolett.0c02956.

[9] T. Li, P.F. Ibáñez-Ibáñez, V. Håkonsen, J. Wu, K. Xu, Y. Zhuo, S. Luo, J. He, Z. Zhang, Self-deicing electrolyte hydrogel surfaces with pa-level ice adhesion and durable antifreezing/antifrost performance, ACS Appl. Mater. Interfaces *12* (31) (2020) 35572–35578, https://doi.org/10.1021/acsami.0c06912.

[10] Z. Mossayebi, V.F. Jafari, P.A. Gurr, R. Simons, G.G. Qiao, Reduced ice adhesion using amphiphilic poly(ionic liquid)-based surfaces, ACS Appl. Mater. Interfaces *15* (5) (2023) 7454–7465, https://doi.org/10.1021/acsami.2c21500.

[11] S. Ozbay, C. Yuceel, H.Y. Erbil, Improved icephobic properties on surfaces with a hydrophilic lubricating liquid, ACS Appl. Mater. Interfaces *7* (39) (2015) 22067–22077, https://doi.org/10.1021/acsami.5b07265.

[12] D.L. Beemer, W. Wang, A.K. Kota, Durable gels with ultra-low adhesion to ice, J. Mater. Chem. A *4* (47) (2016) 18253–18258, https://doi.org/10.1039/c6ta07262c.

[13] F. Chen, Z. Xu, H. Wang, S. Handschuh-Wang, B. Wang, X. Zhou, Bioinspired tough organohydrogel dynamic interfaces enabled subzero temperature antifrosting, deicing, and antiadhesion, ACS Appl. Mater. Interfaces *12* (49) (2020) 55501–55509, https://doi.org/10.1021/acsami.0c17163.

[14] Z. Fu, H. Liu, Q. Lyu, J. Dai, C. Ji, Y. Tian, Anti-freeze hydrogel-based sensors for intelligent wearable human-machine interaction, Chem. Eng. J. *481* (2024), https://doi.org/10.1016/j.cej.2024.148526.

[15] Y. Gao, J. Peng, M. Zhou, Y. Yang, X. Wang, J. Wang, Y. Cao, W. Wang, D. Wu, A multi-model, large range and anti-freezing sensor based on a multi-crosslinked poly(vinyl alcohol) hydrogel for human-motion monitoring, J. Mater. Chem. B *8* (48) (2020) 11010–11020, https://doi.org/10.1039/d0tb02250k.

[16] Q. Guo, Z. He, Y. Jin, S. Zhang, S. Wu, G. Bai, H. Xue, Z. Liu, S. Jin, L. Zhao, J. Wang, Tuning ice nucleation and propagation with counterions on multilayer hydrogels, Langmuir *34* (40) (2018) 11986–11991, https://doi.org/10.1021/acs.langmuir.8b02106.

[17] X. Hou, L. Lin, K. Li, F. Jiang, D. Qiao, B. Zhang, F. Xie, Towards superior biopolymer gels by enabling interpenetrating network structures: a review on types, applications, and gelation strategies, Adv. Colloid Interface Sci. (2024) 103113, https://doi.org/10.1016/j.cis.2024.103113.

[18] M. Zhu, X. Wang, H. Tang, J. Wang, Q. Hao, L. Liu, Y. Li, K. Zhang, O.G. Schmidt, Antifreezing hydrogel with high zinc reversibility for flexible and durable aqueous batteries by cooperative hydrated cations, Adv. Funct. Mater. *30* (6) (2020), https://doi.org/10.1002/adfm.201907218.

[19] M. Ewert, J.W. Deming, Sea ice microorganisms: environmental constraints and extracellular responses, Biology *2* (2) (2013) 603–628, https://doi.org/10.3390/biology2020603.

[20] C. Krembs, H. Eicken, K. Junge, J.W. Deming, High concentrations of exopolymeric substances in Arctic winter sea ice: implications for the polar ocean carbon cycle and cryoprotection of diatoms, Deep-Sea Res. I *49* (2002) 2163–2181, https://doi.org/10.1016/S0967-0637(02)00122-X.

[21] H. Yoshida, T. Hatakeyama, H. Hatakeyama, Characterization of water in polysaccharide hydrogels by DSC, J. Therm. Anal. *40* (1992) 483–489.

[22] K.A. Emelyanenko, A.M. Emelyanenko, L.B. Boinovich, Review of the state of the art in studying adhesion phenomena at interfaces of solids with solid and liquid aqueous media, Colloid J. *84* (3) (2022) 265–286, https://doi.org/10.1134/S1061933X22030036.

[23] M. Chen, W. Wang, J. Fang, P. Guo, X. Liu, G. Li, Z. Li, X. Wang, J. Li, K. Lei, Environmentally adaptive polysaccharide-based hydrogels and their applications in extreme conditions: a review, Int. J. Biol. Macromol. *241* (2023), https://doi.org/10.1016/j.ijbiomac.2023.124496.

[24] I. Tagliaro, G. Musile, P. Caricato, R.M. Dorizzi, F. Tagliaro, C. Antonini, Chitosan film sensor for ammonia detection in microdiffusion analytical devices, Polymers *15* (21) (2023), https://doi.org/10.3390/polym15214238.

[25] E. Zhu, H. Xu, Y. Xie, Y. Song, D. Liu, Y. Gao, Z. Shi, Q. Yang, C. Xiong, Antifreezing ionotronic skin based on flexible, transparent, and tunable ionic conductive nanocellulose hydrogels, Cellulose *28* (9) (2021) 5657–5668, https://doi.org/10.1007/s10570-021-03878-8.

[26] L. Shu, Z. Wang, X.F. Zhang, J. Yao, Highly conductive and anti-freezing cellulose hydrogel for flexible sensors, Int. J. Biol. Macromol. *230* (2023), https://doi.org/10.1016/j.ijbiomac.2023.123425.

[27] R. Tong, G. Chen, D. Pan, J. Tian, H. Qi, R. Li, F. Lu, M. He, Ultrastretchable and antifreezing double-cross-linked cellulose ionic hydrogels with high strain sensitivity under a broad range of temperature, ACS Sustain. Chem. Eng. *7* (16) (2019) 14256–14265, https://doi.org/10.1021/acssuschemeng.9b03555.

[28] L. Cao, Z. Zhao, X. Wang, X. Huang, J. Li, Y. Wei, Tough, Antifreezing, and Conductive Hydrogel Based on Gelatin and Oxidized Dextran, Adv. Mater. Technol. *7* (7) (2022), https://doi.org/10.1002/admt.202101382.

[29] Y. Gao, F. Jia, G. Gao, Ultra-thin, transparent, anti-freezing organohydrogel film responded to a wide range of humidity and temperature, Chem. Eng. J. *430* (2022), https://doi.org/10.1016/j.cej.2021.132919.

[30] J. Chen, Z. Luo, Q. Fan, J. Lv, J. Wang, Anti-Ice coating inspired by ice skating, Small *10* (22) (2014) 4693–4699, https://doi.org/10.1002/smll.201401557.

[31] B. Huang, S. Jiang, Y. Diao, X. Liu, W. Liu, J. Chen, H. Yang, Hydrogels as durable anti-icing coatings inhibit and delay ice nucleation, Molecules *25* (15) (2020), https://doi.org/10.3390/molecules25153378.

[32] J. Nie, Z. Wang, Q. Hu, Difference between chitosan hydrogels via alkaline and acidic solvent systems, Sci. Rep. *6* (2016), https://doi.org/10.1038/srep36053.

[33] C. Li, Q. Han, Y. Guan, Y. Zhang, Thermal gelation of chitosan in an aqueous alkali-urea solution, Soft Matter *10* (41) (2014) 8245–8253, https://doi.org/10.1039/c4sm01336k.

[34] Z. Lu, L. Zou, X. Zhou, D. Huang, Y. Zhang, High strength chitosan hydrogels prepared from NaOH/urea aqueous solutions: the role of thermal gelling, Carbohydr. Polym. *297* (2022), https://doi.org/10.1016/j.carbpol.2022.120054.

[35] J. Duan, X. Liang, Y. Cao, S. Wang, L. Zhang, High strength chitosan hydrogels with biocompatibility via new avenue based on constructing nanofibrous architecture, Macromolecules *48* (8) (2015) 2706–2714, https://doi.org/10.1021/acs.macromol.5b00117.

[36] Z. Wang, J. Nie, W. Qin, Q. Hu, B.Z. Tang, Gelation process visualized by aggregation-induced emission fluorogens, Nat. Commun. *7* (2016), https://doi.org/10.1038/ncomms12033.

[37] R. Ladiè, C. Cosentino, I. Tagliaro, C. Antonini, G. Bianchini, S. Bertini, Supramolecular structuring of hyaluronan-lactose-modified chitosan matrix: Towards high-performance biopolymers with excellent biodegradation, Biomolecules *11* (3) (2021) 1–19, https://doi.org/10.3390/biom11030389.

[38] S. Petroni, I. Tagliaro, C. Antonini, M. D'Arienzo, S.F. Orsini, J.F. Mano, V. Brancato, J. Borges, L. Cipolla, Chitosan-Based Biomaterials: Insights into Chemistry, Properties, Devices, and Their Biomedical Applications Multidisciplinary Digital Publishing Institute (MDPI) , Vol. 21 In Marine Drugs2023, , 10.3390/md21030147.

[39] N.M. Porpiglia, I. Tagliaro, B. Pellegrini, A. Alessi, F. Tagliaro, L. Russo, F. Cadamuro, G. Musile, C. Antonini, S. Bertini, Chitosan derivatives as dynamic coatings for transferrin glycoform separation in capillary electrophoresis, Int. J. Biol. Macromol. *254* (2024), https://doi.org/10.1016/j.ijbiomac.2023.127888.

[40] I. Tagliaro, M. Mariani, R. Akbari, M. Contardi, M. Summa, F. Saliu, R. Nisticò, C. Antonini, PFAS-free superhydrophobic chitosan coating for fabrics, Carbohydr. Polym. *333* (2024), https://doi.org/10.1016/j.carbpol.2024.121981.

[41] I. Tagliaro, S. Seccia, B. Pellegrini, S. Bertini, C. Antonini, Chitosan-based coatings with tunable transparency and superhydrophobicity: a solvent-free and fluorine-free approach by stearoyl derivatization, Carbohydr. Polym. *302* (2023), https://doi.org/10.1016/j.carbpol.2022.120424.

[42] J. Cai, L. Zhang, Unique gelation behavior of cellulose in NaOH/urea aqueous solution, Biomacromolecules *7* (1) (2006) 183–189, https://doi.org/10.1021/bm0505585.

[43] Y. Fang, R. Zhang, B. Duan, M. Liu, A. Lu, L. Zhang, Recyclable universal solvents for chitin to chitosan with various degrees of acetylation and construction of robust hydrogels, ACS Sustain. Chem. Eng. *5* (3) (2017) 2725–2733, https://doi.org/10.1021/acssuschemeng.6b03055.

[44] G. Ru, S. Wu, X. Yan, B. Liu, P. Gong, L. Wang, J. Feng, Inverse solubility of chitin/chitosan in aqueous alkali solvents at low temperature, Carbohydr. Polym. *206* (2019) 487–492, https://doi.org/10.1016/j.carbpol.2018.11.016.

[45] S. Liu, L. Li, Unique gelation of chitosan in an alkali/urea aqueous solution, Polymer *141* (2018) 124–131, https://doi.org/10.1016/j.polymer.2018.03.012.

[46] B. Xiong, P. Zhao, K. Hu, L. Zhang, G. Cheng, Dissolution of cellulose in aqueous NaOH/urea solution: role of urea, Cellulose *21* (3) (2014) 1183–1192, https://doi.org/10.1007/s10570-014-0221-7.

[47] L. Stendardo, G. Gastaldo, M. Budinger, V. Pommier-Budinger, I. Tagliaro, P. F. Ibáñez-Ibáñez, C. Antonini, Reframing ice adhesion mechanisms on a solid surface, Appl. Surf. Sci. *641* (2023), https://doi.org/10.1016/j.apsusc.2023.158462.

[48] R. Akbari, C. Antonini, Contact angle measurements: From existing methods to an open-source tool Elsevier B.V, Advances in Colloid and Interface Science 294 (2021), https://doi.org/10.1016/j.cis.2021.102470.

[49] J. Ostrowska-Czubenko, M. Pieróg, M. Gierszewska-Drużyńska, State of water in noncrosslinked and crosslinked hydrogel chitosan membranes - DSC studies, Prog. Chem. Appl. Chitin Its Deriv. *Vol. XVI* (2011) 147–156.

[50] T. Wang, S. Gunasekaran, State of water in chitosan-PVA hydrogel, J. Appl. Polym. Sci. *101* (5) (2006) 3227–3232, https://doi.org/10.1002/app.23526.

[51] L. Gao, H. Gan, Z. Meng, R. Gu, Z. Wu, L. Zhang, X. Zhu, W. Sun, J. Li, Y. Zheng, G. Dou, Effects of genipin cross-linking of chitosan hydrogels on cellular adhesion and viability, Colloids Surf. B: Biointerfaces *117* (2014) 398–405, https://doi.org/10.1016/j.colsurfb.2014.03.002.

[52] R. Digilov, Charge-induced modification of contact angle: the secondary electrocapillary effect, Langmuir *16* (16) (2000) 6719–6723, https://doi.org/10.1021/la991308a.

[53] T. Bharathidasan, S.V. Kumar, M.S. Bobji, R.P.S. Chakradhar, B.J. Basu, Effect of wettability and surface roughness on ice-adhesion strength of hydrophilic, hydrophobic and superhydrophobic surfaces, Appl. Surf. Sci. *314* (2014) 241–250, https://doi.org/10.1016/j.apsusc.2014.06.101.

[54] A. Dotan, H. Dodiuk, C. Laforte, S. Kenig, The relationship between water wetting and ice adhesion, J. Adhes. Sci. Technol. *23* (15) (2009) 1907–1915, https://doi.org/10.1163/016942409X12510925843078.
[55] W. Lin, D. Dalmazzone, W. Fürst, A. Delahaye, L. Fournaison, P. Clain, Accurate DSC measurement of the phase transition temperature in the TBPB-water system, J. Chem. Thermodyn. *61* (2013) 132–137, https://doi.org/10.1016/j.jct.2013.02.005.
[56] N.J. Chen, J. Morikawa, T. Hashimoto, Effect of amino acids on the eutectic behavior of NaCl solutions studied by DSC, Cryobiology *50* (3) (2005) 264–272, https://doi.org/10.1016/j.cryobiol.2005.02.004.
[57] P. Tompa, K.H. Han, M. Bokor, P. Kamasa, Á. Tantos, B. Fritz, D.H. Kim, C. Lee, T. Verebélyi, K. Tompa, Wide-line NMR and DSC studies on intrinsically disordered p53 transactivation domain and its helically pre-structured segment, BMB Rep. *49* (9) (2016) 497–501, https://doi.org/10.5483/BMBRep.2016.49.9.037.
[58] M.F. Queiroz, K.R.T. Melo, D.A. Sabry, G.L. Sassaki, H.A.O. Rocha, Does the use of chitosan contribute to oxalate kidney stone formation, Mar. Drugs *13* (1) (2015) 141–158, https://doi.org/10.3390/md13010141.
[59] G. Stojkov, Z. Niyazov, F. Picchioni, R.K. Bose, Relationship between structure and rheology of hydrogels for various applications, Gels *7* (4) (2021), https://doi.org/10.3390/gels7040255.
[60] L. Zhao, L. Niu, H. Liang, H. Tan, C. Liu, F. Zhu, PH and glucose dual-responsive injectable hydrogels with insulin and fibroblasts as bioactive dressings for diabetic wound healing, ACS Appl. Mater. Interfaces *9* (43) (2017) 37563–37574, https://doi.org/10.1021/acsami.7b09395.
[61] M.L. Tummino, R. Nisticò, C. Riedo, D. Fabbri, M. Cerruti, G. Magnacca, Waste cleaning waste: combining alginate with biowaste-derived substances in hydrogels and films for water cleanup, Chem. - A Eur. J. *27* (2) (2021) 660–668, https://doi.org/10.1002/chem.202003250.
[62] Y. Zhao, Z. Li, Q. Li, L. Yang, H. Liu, R. Yan, L. Xiao, H. Liu, J. Wang, B. Yang, Q. Lin, Transparent conductive supramolecular hydrogels with stimuli-responsive properties for on-demand dissolvable diabetic foot wound dressings, Macromol. Rapid Commun. *41* (24) (2020), https://doi.org/10.1002/marc.202000441.
[63] Z. He, Y. Zhuo, Z. Zhang, J. He, Design of icephobic surfaces by lowering ice adhesion strength: a mini review, Coatings *11* (11) (2021), https://doi.org/10.3390/coatings11111343.
[64] N. Rehfeld, J.D. Brassard, M. Yamazaki, H. Sakaue, M. Balordi, H. Koivuluoto, J. Mora, J. He, M.L. Pervier, A. Dolatabadi, E. Asenath-Smith, M. Järn, X. Hou, V. Stenzel, Round-robin study for ice adhesion tests, Aerospace *11* (2) (2024), https://doi.org/10.3390/aerospace11020106.